IOP PUBLISHING EUROPEAN JOURNAL OF PHYSICS

Eur. J. Phys. **31** (2010) 775–784 doi:10.1088/0143-0807/31/4/007

Soccer ball lift coefficients via trajectory analysis

John Eric Goff[1] **and Matt J Carré**[2]

[1] Department of Physics, Lynchburg College, Lynchburg, VA 24501, USA
[2] Department of Mechanical Engineering, University of Sheffield, Sheffield S1 3JD, UK

E-mail: goff@lynchburg.edu

Received 10 March 2010, in final form 15 April 2010
Published 14 May 2010
Online at stacks.iop.org/EJP/31/775

Abstract

We performed experiments in which a soccer ball was launched from a machine while two high-speed cameras recorded portions of the trajectory. Using the trajectory data and published drag coefficients, we extracted lift coefficients for a soccer ball. We determined lift coefficients for a wide range of spin parameters, including several spin parameters that have not been obtained by today's wind tunnels. Our trajectory analysis technique is not only a valuable tool for professional sports scientists, it is also accessible to students with a background in undergraduate-level classical mechanics.

1. Introduction

We recently published a paper [1] that describes how one may extract a soccer ball's drag and lift coefficients from trajectory analysis. Prior to our work, researchers investigated soccer ball aerodynamics using wind tunnels [2–5] and computer models [6–11]. Trajectory analysis work has been performed in other sports like tennis [12, 13] and baseball [14, 15]. Besides acting as a technique complementary to wind-tunnel experiments, trajectory analysis allows for the study of the aerodynamics of projectiles for researchers without access to expensive wind tunnel machines. Trajectory analysis is also a valuable tool for examining aerodynamic coefficients in parameter ranges not currently studied by modern wind tunnels. Our technique is accessible to undergraduate and graduate science and engineering students looking to analyse trajectories of rotating objects moving through fluids.

The two main aerodynamic parameters used in trajectory analysis are the Reynolds number, Re, and the spin parameter, Sp. The Reynolds number is a measure of the relative sizes of the inertial and viscous forces on the ball and is defined as [16] $Re = vD/\nu$, where v is the ball's speed, D is the ball's diameter and ν is the kinematic viscosity, which is the ratio of viscosity to air density. We studied the Adidas Teamgeist ball, which was introduced in the 2006 World Cup, for which we measured $D \simeq 0.218\,\mathrm{m}$. With $\nu \simeq 1.54 \times 10^{-5}\,\mathrm{m^2\ s^{-1}}$, the conversion between the Reynolds number and the soccer ball speed is $Re \times 10^{-5} \simeq v/(7\,\mathrm{m\ s^{-1}})$. Soccer is played essentially in the range $70\,000 < Re < 490\,000$.

The spin parameter is defined as $Sp = r\omega/v$ and measures the ratio of the rotating ball's tangential speed at the equator to its centre-of-mass speed with respect to the air [17]. Here, r is the ball's radius and ω is the angular speed. Wind tunnel experiments [2–5] investigated spin parameters as high as 0.3 or so. Our trajectory analysis work allows for spin parameters as high as about 1.0 because unlike wind tunnels, we can work with low speeds and high spin rates just as easily as other combinations of speed and spin.

2. Trajectory analysis technique

In this section we provide a summary of our trajectory analysis technique. For more details, as well as access to sample computer codes, we refer the reader to our first paper [1].

2.1. Soccer ball flight physics

While in the air, a soccer ball experiences a gravitational force from the Earth and a force from the air through which it traverses. The gravitational force is $\vec{F}_g = m\,\vec{g}$, where the Teamgeist ball's mass is $m = 0.436\,\mathrm{kg}$ and the acceleration due to gravity has magnitude $g = 9.8\,\mathrm{m\ s^{-2}}$. The ball's weight, $m\,g \simeq 4.28\,\mathrm{N}$, was taken to be constant.

Though the air exerts a single force on the ball, we take the conventional approach of splitting that air force into a component called 'drag' and a component called 'lift'. The drag force is in the direction opposite to the ball's velocity, $\vec{v}$, and has magnitude [18]

$$F_D = \tfrac{1}{2}\rho A v^2 C_D. \tag{1}$$

A ball spinning with an angular velocity $\vec{\omega}$ experiences a lift (or Magnus [19]) force in the direction of $\vec{\omega} \times \vec{v}$ with magnitude [18]

$$F_L = \tfrac{1}{2}\rho A v^2 C_L. \tag{2}$$

Equations (1) and (2) require the air density, $\rho = 1.2\,\mathrm{kg\,m^{-3}}$, and the ball's cross-sectional area, $A \simeq 0.0375\,\mathrm{m^2}$.

Also needed in equations (1) and (2) are the drag and lift coefficients, C_D and C_L, respectively. These aerodynamic coefficients are, in general, functions of both *Re* and *Sp*. For C_D, we made use of wind-tunnel experiments [3] on Teamgeist soccer balls. The goal of this work is to obtain C_L for various *Re* and *Sp*.

Figure 1 shows the experimental data [3] we used for C_D. We note that the data shown in that figure are for balls with no spin. So that we could extract C_D values for speeds that do not coincide with data points, we created a fitting function ([11], see also [20][3]) given by

$$C_D = a + \frac{b}{1 + \exp[(v - v_c)/v_s]}, \tag{3}$$

where $a = 0.155$, $b = 0.346$, $v_c = 12.19\,\mathrm{m\ s^{-1}}$ and $v_s = 1.309\,\mathrm{m\ s^{-1}}$. Figure 1 illustrates a general feature of the drag coefficient for spherical objects, namely a roughly factor-of-two drop during the transition from laminar flow to turbulent flow at a critical speed close to v_c [19].

The drag coefficient increases as spin is imparted to a ball. Figure 2 shows wind-tunnel results [3] for the drag coefficient as a function of the spin parameter. Note that wind-tunnel results do not go beyond $Sp \simeq 0.3$; also note that the five tests shown in figure 2 were all conducted at speeds greater than the critical speed. The amount of experimental data available for *Sp*-dependent C_D are thus limited to post-critical speeds with spin parameters such that $0.05 < Sp < 0.3$. Given that limitation, we use the wind-tunnel data to extrapolate values of

[3] We first saw the form equation (3) in this book for a baseball's drag coefficient.

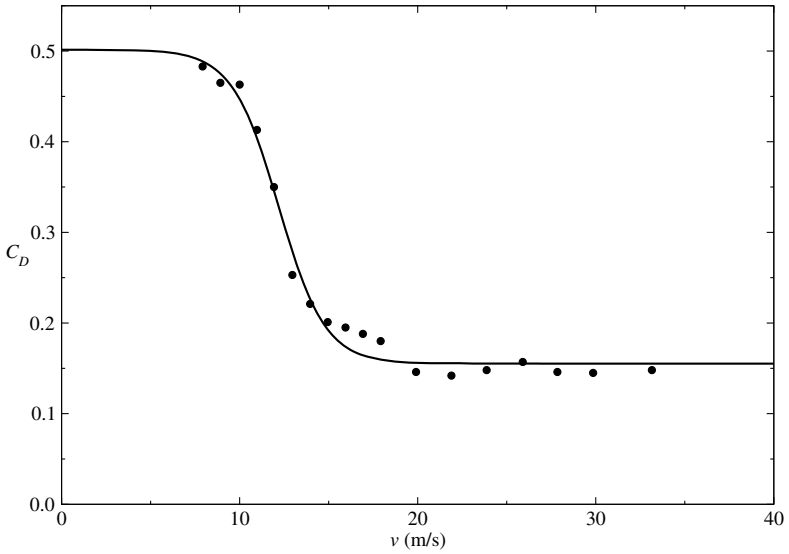

Figure 1. Experimental wind-tunnel data (points) for C_D for non-spinning Teamgeist soccer balls from [3]. A fit (curve) to the data is given by equation (3).

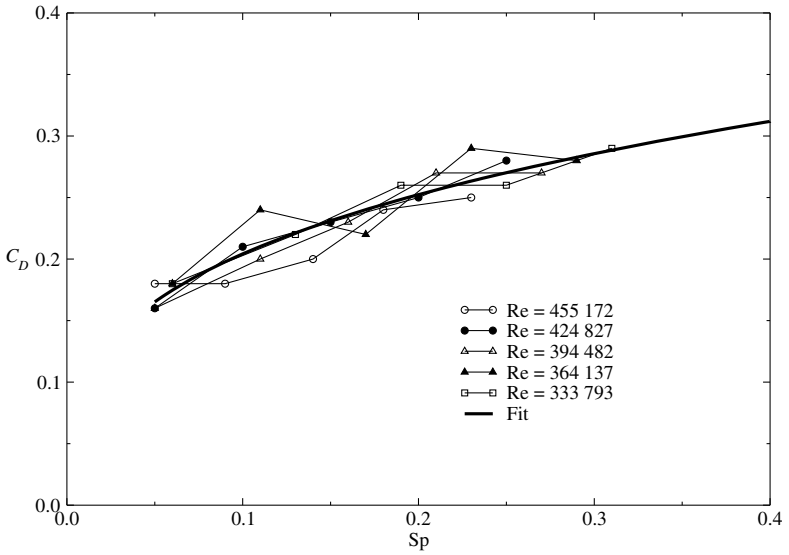

Figure 2. Experimental wind-tunnel data from [3] for C_D as a function of Sp. Note that all five Reynolds numbers are above the critical speed. Lines between data points help visually separate the five experiments. The thick line represents the fit given by equation (4).

C_D for $Sp > 0.3$. Because C_D does not appear to depend strongly on Re above the critical speed, we use one fitting function given by

$$C_D = c\, Sp^d, \tag{4}$$

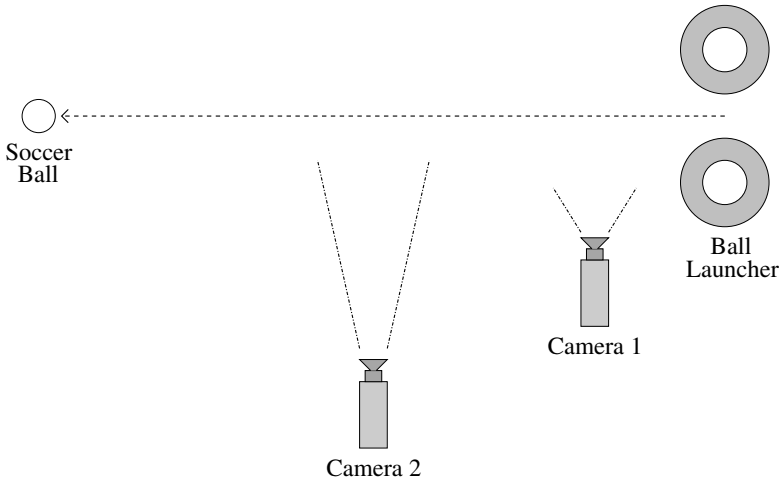

Figure 3. A not-to-scale sketch of our experimental setup. Camera 1, about 1.5 m from the plane of the trajectory, recorded the launch of the soccer ball. Camera 2, about 13 m from the plane of the trajectory, recorded a portion of the trajectory near the apex of the flight.

where $c = 0.4127$ and $d = 0.3056$. The above is used for $v > v_c$ and $Sp > 0.05$. For $v < v_c$ and/or $Sp < 0.05$, we use equation (3). We note, however, that for all the work put into estimating C_D as a function of speed and spin parameter, the lift coefficients we extract via trajectory analysis do not depend strongly on the choice of C_D.

2.2. Experimental setup

The sports hall at the University of Sheffield was the venue for our trajectory experiments. Using a ball launcher, which employs four counter-rotating wheels that allow for variations in launch speed and initial spin, we tested a wide range of Reynolds numbers and spin parameters. Figure 3 shows a schematic of our experimental setup. We employed high-speed cameras set to record 1000 frames per second.

Though camera 2 allowed us to record a portion of the ball's trajectory near its apex, we needed only the part of the trajectory recorded by camera 1 to extract lift coefficients. The reason is that camera 1 records roughly the first 0.07 s of the ball's trajectory during which the Reynolds number and the spin parameter do not vary appreciably. Our high-speed cameras produce movies in a cine format. Phantom software's *Cine Viewer* was used to convert a cine to AVI format. In-house software[4] was then used to track the ball and obtain Cartesian coordinates of the ball's centre of mass. Figure 4 shows a typical trajectory for a Teamgeist ball with backspin.

We determined the spin rate by following a given point on the ball as the ball turned either a half turn (for slow spins) or a full turn (for fast spins). We examined Teamgeist launches for spin rates as small as about 5.8 rad s^{-1} (55 rpm) to spin rates as large as about 112 rad s^{-1} (1070 rpm).

[4] Our in-house software was developed by Richard Dignall and Simon Goodwill at the University of Sheffield. There are other commercially available software packages that allow one to analyse trajectories from movies. A good one sold primarily in the USA is *VideoPoint*.

Figure 4. Data from camera 1 for a launch with backspin. Each circle's centre denotes the ball's centre of mass in 0.005 s intervals. The ball was launched with the speed of 15.8 m s^{-1} at an angle of 27.2° above the horizontal. Its 84.9 rad s^{-1} (811 rpm) angular speed meant that $Sp \simeq 0.59$. (This figure is in colour only in the electronic version)

2.3. Lift coefficient extraction

Once we have analysed a given camera 1 movie, we have a set of Cartesian coordinates for the first 0.07 s of the ball's trajectory. We then need to match those experimental data to a numerical solution of Newton's second law.

Figure 5 shows a free-body diagram of the soccer ball in flight with the gravitational, drag and lift forces acting on the ball. Using the free-body diagram, we set up Newton's second law as

$$m\vec{a} = \vec{F}_g + \vec{F}_D + \vec{F}_L, \tag{5}$$

where $\vec{a}$ is the Teamgeist ball's linear acceleration. Equation (5) is a second-order nonlinear differential equation. The speed dependence of the drag and lift forces means that the components of equation (5) are coupled. Such an equation can only be solved with the help of a computer.

We fit a computational solution of equation (5) to the camera 1 data with a lift coefficient chosen to minimize the least-squares deviation between the data and the computational fit. Because *Re* and *Sp* hardly change during the time that camera 1 records, we are able to state a lift coefficient for a specific *Re* and *Sp*.

Figure 6 shows wind-tunnel data [3] for C_L as well as trajectory analysis results [1] for C_L for a 32-panel soccer ball. Though we distinguish between backspin ($C_L > 0$) and topspin ($C_L < 0$) in our computer codes, the physical manifestation of the air force's component perpendicular to drag is independent of whether the ball has backspin or topspin. We are thus interested only in the absolute value of C_L.

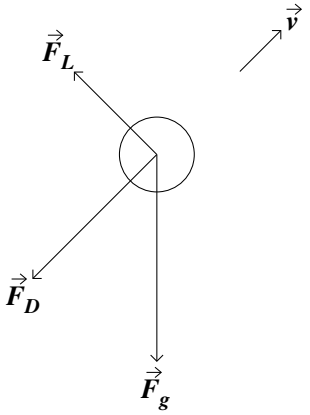

Figure 5. The forces on a soccer ball. The gravitational force points down; the drag force is opposite to the ball's velocity; the lift force is perpendicular to the ball's velocity (shown here for a ball with backspin) and in the plane formed by the velocity and the ball's weight. A sideways force is possible if the spin axis is not perpendicular to the plane of this page.

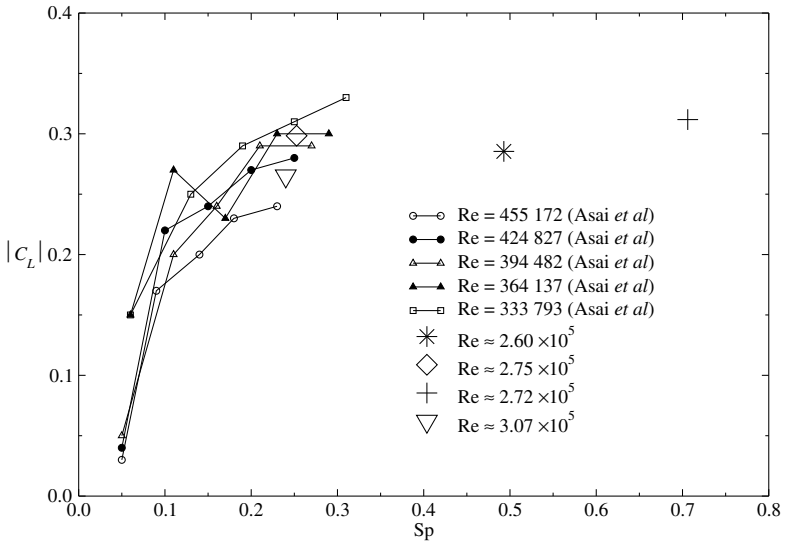

Figure 6. Experimental wind-tunnel data for $|C_L|$ from [3] as a function of Sp. Also shown are four data points from our trajectory analysis work on 32-panel soccer balls in [1]. Lines between data points visually separate wind-tunnel data from our trajectory analysis results.

3. Results and discussion

Our initial work [1] concentrated on the technique of using trajectory analysis to extract aerodynamic coefficients. In that work, we contributed four points to figure 6, two consistent with the previous wind-tunnel work [3] and two associated with values of Sp beyond where current wind tunnels test.

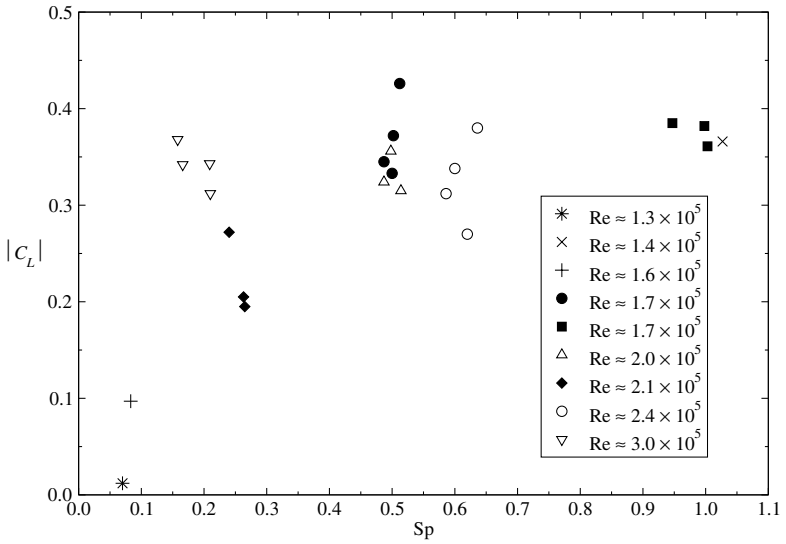

Figure 7. Our trajectory analysis lift coefficient results for a Teamgeist soccer ball. Each Reynolds number in the legend represents the average Reynolds number for a given subset of data.

Having established the method of extraction of C_L from trajectory analysis, we now present results for the Teamgeist soccer ball for several spin parameters. Figure 7 shows the main result of this work. With the exception of three trials (two at small *Sp* and one at large *Sp*), we performed three or four tests at each speed and spin setting on our ball launcher. The Reynolds numbers given in the graph legend represent average values of *Re* for each subset of data. The Reynolds number for any given test is not more than a couple of per cent off from the stated average.

We remind the reader that $Re = 2 \times 10^5$ corresponds to a speed of about 14 m s^{-1} (or about 31.5 miles per hour). Large spin parameters correspond to low-speed, high-spin kicks in the game of soccer. A typical David Beckham free kick with lots of sidespin has $Re \simeq 5 \times 10^5$ and $Sp = 0.2$ [1]. The University of Sheffield sports hall's size limits our ability to study balls launched at Reynolds numbers greater than about 3×10^5. Balls launched at greater speeds collide with the sports hall's rafters or far wall. Studying larger Reynolds-number launches would require us to set up a net or other stopping device just past the region filmed by camera 1. We may pursue such an experiment in the future.

There is much to be gleaned from figure 7. Note that there is some spread in data corresponding to roughly the same Reynolds number. We believe that spread arises from a couple of sources. The first source is the ball itself. Though we tried to launch the ball with the same starting orientation for each test, we noticed slight variations in the ball's orientation each time it exited our launcher. The Teamgeist ball's surface comprises 14 thermally bonded panels. It is known [19] that the surface roughness alters the way in which the boundary layer separates from the ball. Changes in the ball's orientation from one test to another could easily lead to changes in the way the boundary layer separates from the ball, thus leading to differences in the lift force. To quantify this effect, we would need to devise an experiment, either with a wind tunnel or with another approach, that would allow for visualization of the boundary-layer separation.

A second possible source for the spread in the C_L data is the procedure by which we obtain the ball's coordinates during the time camera 1 films. As figure 4 shows, we use a circle's centre to locate the ball's centre of mass in each frame. The procedure for extracting the lift coefficient is sensitive to the centre-of-mass coordinates obtained by camera 1. By 'sensitive', we mean that the value of C_L could easily change by a factor of 2 if one is not careful to align our in-house software circle's centre with the centre of the ball. Given that level of sensitivity, we analyse a given camera 1 movie several times, each time using our in-house software to obtain the ball's centre-of-mass coordinates. We then average those sets of coordinates and determine C_L from the average set. The number of times we need to analyse a given movie depends on how quickly the computed C_L settles to a stable value. We usually need to average three to eight sets of coordinates to get a stable C_L. We feel this procedure helps eliminate errors we introduced while trying to determine the location of the ball's centre of mass in each frame of the camera 1 movie.

As for the physics content in figure 7, we see that as the spin parameter increases, the lift coefficient appears to level off (we certainly cannot apply that conclusion for $Sp > 1$, where we have no data). We noted that trend with our work on 32-panel balls (see figure 6).

To understand why C_L does not increase at the same rate for $0.5 < Sp < 1$ as it does for $0 < Sp < 0.5$, we look on the opposite sides of the ball and examine the speed of the air relative to the ball's surface. The sketch in figure 5 shows a ball with backspin because the lift force has a vertical component. If the ball is spinning with an angular speed ω and moving with the centre-of-mass speed v, the relative air speed near the top of the ball (where the $\vec{F}_L$ vector emerges from the ball in figure 5) is roughly $v - r\omega$, were r is the ball's radius. On the opposite side of the ball, the relative air speed is roughly $v + r\omega$. We use the word 'roughly' because in the ball's reference frame, the speed of the air rises from zero at the ball's surface to nearly the free-stream speed just outside the boundary layer. But, using $v \pm r\omega$ gives us an idea of what might make C_L level off for $0.5 < Sp < 1$. We can validate this idea with our camera 1 movies. For $Sp \simeq 1$, meaning $v - r\omega \simeq 0$, the ball in the camera 1 movie appears to roll without slipping on an invisible inclined plane. With backspin, such a movie is strange to watch because the invisible inclined plane is above the ball!

Now, as the spin rate increases for a given centre-of-mass speed, $v - r\omega$ decreases, meaning it may decrease below the critical speed, v_c. If the ball spins fast enough, the $v - r\omega$ side of the ball will experience a laminar boundary layer separation, while the $v + r\omega$ side has a turbulent boundary layer separation. Because laminar separation does not occur as far back on the ball as turbulent separation [19], the $v - r\omega$ side of the ball does not whip the air around as much as it would if the separation were turbulent. If top of the ball in figure 5 has laminar flow because $v - r\omega < v_c$, air will not be whipped downwards as much as if the top of the ball had turbulent separation. That makes for smaller lift in the former case compared to the latter.

To better understand this idea, consider the side of the ball with a relative air speed given by $v - r\omega$. If $v - r\omega < v_c$, we may expect laminar separation on that side of the ball. Because $Sp = r\omega/v$, we write the aforementioned condition as

$$Re < \frac{Re_c}{1 - Sp}, \tag{6}$$

where speeds have been changed to Reynolds numbers. One may estimate the critical Reynolds number, Re_c, from the estimate of the critical speed required to make the fit in equation (3). With $v_c = 12.19\,\mathrm{m\,s^{-1}}$, $Re_c \simeq 1.73 \times 10^5$, which is a good enough estimate for what we are doing here. We can now plot Re versus Sp using equation (6) to see which combinations of Re and Sp lead to the possibility of laminar separation on one side of the ball while there is turbulent separation on the other side. We also note that the condition $v + r\omega < v_c$ means

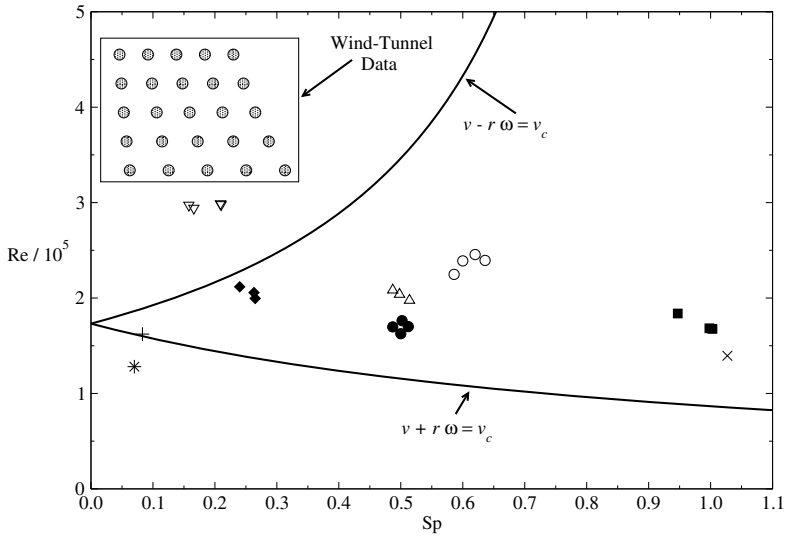

Figure 8. Reynolds number versus spin parameter. The two curves represent $v \pm r\omega = v_c$. The boxed data in the upper-left corner are from [3] and figure 6. The rest of the data represent our Teamgeist data from figure 7 (same symbols).

that both sides of the ball experience laminar separation. We can plot that condition simply by changing the minus sign in the denominator of equation (6) to a plus sign.

Figure 8 shows a plot of Reynolds number versus spin parameter with two curves drawn to show where $v \pm r\omega = v_c$. Above the top curve, both sides of the ball have turbulent separation. Below the bottom curve, both sides of the ball have laminar separation. Between the two curves, the $v - r\omega$ side of the ball has laminar separation while the $v + r\omega$ side of the ball has turbulent separation. We emphasize that the two curves shown in figure 8 are merely approximations of where transitions between laminar flow and turbulent flow exist. Such transitions are certainly not instantaneous at a specific, critical speed. Figure 8 provides a rough idea of where the three cases exist.

To figure 8 we have also added wind-tunnel data from [3] that appeared in figure 6, as well as our Teamgeist data from figure 7. Note that all of the wind-tunnel data were taken at large enough *Re* and small enough *Sp* that both sides of the ball likely experienced turbulent separation. Just one set of our data, for $Re \simeq 3 \times 10^5$, sits in that region. Our two low-spin tests are either in or just slightly above the region associated with both sides of the ball having laminar separation. The rest of our tests fell in the middle region. It is thus no surprise to us that the C_L values in figure 7 level off as *Sp* increases.

The preceding discussion helps us understand why C_D increases with *Sp*, as seen in figure 2. A ball with $v - r\omega < v_c$ on one side does not whip air around it as well as if it had turbulent separation on that side. The net force from the air thus has a slightly greater drag component. As we mentioned earlier, there is just one force on the ball from the air. Transitions from turbulent to laminar on one side of the ball at high *Sp* appear to result in one force component becoming a little larger while the other becomes a little smaller. Even for $Sp < 0.3$, where the data in figure 2 were taken, some portion of the whipped air will be along the direction of the drag force.

We finally make a couple of quick comparisons between figures 6 and 7. The Teamgeist's $|C_L|$ for $Re \simeq 3.0 \times 10^5$ and $Sp \simeq 0.2$ is clearly larger than the corresponding $|C_L|$ for the 32-panel ball. Also, the Teamgeist $|C_L|$ results we have for the range $0.5 < Sp < 0.7$ are larger than the two $|C_L|$ values we have in that range for the 32-panel ball. For a fully quantitative comparison between the 32-panel ball and the Teamgeist ball, we would require more lift data for the 32-panel ball, especially for $Sp > 0.3$. But, a comparison between figures 6 and 7 suggests that the Teamgeist's $|C_L|$ is slightly larger than the 32-panel ball's $|C_L|$.

We hope to apply our trajectory analysis technique to the Adidas Jabulani ball, which is to be used for the 2010 World Cup in South Africa. That ball has eight thermally bonded panels and a grooved surface. It will be interesting to see how C_D and C_L values for that ball compare to the Teamgeist ball.

Acknowledgments

One of us (JEG) thanks the University of Sheffield's *Bridging the Gaps* fellowship program for financial support.

References

[1] Goff J E and Carré M J 2009 Trajectory analysis of a soccer ball *Am. J. Phys.* **77** 1020–7
[2] Carré M J, Goodwill S R and Haake S J 2005 Understanding the effect of seams on the aerodynamics of an association football *J. Mech. Eng. Sci.* **219** 657–66
[3] Asai T, Seo K, Kobayashi O and Sakashita R 2007 Fundamental aerodynamics of the soccer ball *Sports Eng.* **10** 101–10
[4] Barber S 2007 The aerodynamics of association footballs *PhD Thesis* University of Sheffield (unpublished)
[5] Passmore M A, Tuplin S, Spencer A and Jones R 2008 Experimental studies of the aerodynamics of spinning and stationary footballs *J. Mech. Eng. Sci.* **222** 195–205
[6] Carré M J, Akatsuka T and Haake S J 2002 The curve kick of a football: II. Flight through the air *Sports Eng.* **5** 193–200
[7] Wesson J 2002 *The Science of Soccer* (Bristol: Institute of Physics Publishing)
[8] Bray K and Kerwin D G 2003 Modelling the flight of a soccer ball in a direct free kick *J. Sports Sci.* **21** 75–85
[9] Cook B G and Goff J E 2006 Parameter space for successful soccer kicks *Eur. J. Phys.* **27** 865–74
[10] Barber S, Chin S B and Carré M J 2009 Sports ball aerodynamics: a numerical study of the erratic motion of soccer balls *Comput. Fluids* **38** 1091–100
[11] Goff J E 2010 *Gold Medal Physics: The Science of Sports* (Baltimore, MD: Johns Hopkins University Press) chapter 7
[12] Zayas J M 1986 Experimental determination of the coefficient of drag of a tennis ball *Am. J. Phys.* **54** 622–5
[13] Štěpánek A 1988 The aerodynamics of tennis balls—the topspin lob *Am. J. Phys.* **56** 138–42
[14] Alaways L W and Hubbard M 2001 Experimental determination of baseball spin and lift *J. Sports Sci.* **19** 349–58
[15] Nathan A M 2008 The effect of spin on the flight of a baseball *Am J. Phys.* **76** 119–24
[16] White F M 2008 *Fluid Mechanics* 6th edn (New York: McGraw-Hill) p 27
[17] Tritton D J 1988 *Physical Fluid Dynamics* 2nd edn (Oxford: Clarendon) pp 159–61
[18] De Mestre N 1990 *The Mathematics of Projectiles in Sports* (Cambridge: Cambridge University Press)
[19] Mehta R D 1985 Aerodynamics of sports balls *Ann. Rev. Fluid Mech.* **17** 151–89
[20] Giordano N J and Nakanishi H 2006 *Computational Physics* 2nd edn (Englewood Cliffs, NJ: Prentice-Hall)